Crystal Structure of *Toxoplasma gondii* Hypoxanthine-Guanine Phosphoribosyltransferase with XMP, Pyrophosphate, and Two Mg^{2+} Ions Bound: Insights into the Catalytic Mechanism[†,‡]

Annie Héroux, E. Lucile White, Larry J. Ross, Richard L. Davis,[§] and David W. Borhani*

Drug Discovery Division, Southern Research Institute, Birmingham, Alabama 35205

Received March 3, 1999; Revised Manuscript Received July 14, 1999

ABSTRACT: The crystal structure of the *Toxoplasma gondii* hypoxanthine-guanine phosphoribosyltransferase (HGPRT)−xanthosine 5′-monophosphate (XMP)−pyrophosphate−Mg^{2+} ternary complex has been determined at 1.60 Å resolution. This biproduct, post-transition state structure is of a *T. gondii* HGPRT mutant (Asp150Ala or D150A). The D150A mutant has reduced activity (k_{cat} lower by 11-, 296-, and 8.6-fold for hypoxanthine, guanine, and xanthine, respectively) compared to wild-type *T. gondii* HGPRT. The Michaelis constants for purine bases are altered only slightly, whereas those for α-D-5-phosphoribosyl 1-pyrophosphate (PRPP) are lower by ∼6.5-fold. The ternary complex crystallizes in space group $C222_1$ (a = 55.21 Å, b = 112.25 Å, and c = 144.28 Å) with two subunits in the asymmetric unit; the HGPRT tetramer is completed by the application of 2-fold crystallographic symmetry. All active sites contain XMP {bound in a fashion similar to that of the guanosine 5′-monophosphate (GMP) and inosine 5′-monophosphate (IMP) complexes reported in the preceding article [Héroux, A., et al. (1999) *Biochemistry 38*, 14485−14494]}, pyrophosphate, and two Mg^{2+} ions. Each Mg^{2+} ion is octahedrally coordinated by two terminal pyrophosphate oxygen atoms and several ordered water molecules. This structure shows how HGPRT uses two Mg^{2+} ions to orient and activate the pyrophosphate moiety of PRPP for attack by a purine base, and why mutation in humans of the residue corresponding to Asp206, the only HGPRT amino acid that directly contacts the Mg^{2+} ions, causes Lesch-Nyhan syndrome ($HGPRT_{Kinston}$, D193N). The Leu78−Lys79 peptide bond in the active site adopts the cis configuration, which it must to bind PRPP or pyrophosphate. The contribution of cis−trans isomerization of this peptide bond to the energetics of substrate binding and product release is discussed. A comprehensive description of the HGPRT reaction mechanism is also proposed.

In the preceding article (*1*), we reported the crystal structures of *Toxoplasma gondii* hypoxanthine-guanine phosphoribosyltransferase (HGPRT,[1] EC 2.4.2.8) complexed with its reaction products guanosine 5′-monophosphate (GMP) and inosine 5′-monophosphate (IMP). Here, we present the structure at 1.60 Å resolution of a ternary complex between a *T. gondii* HGPRT active site mutant, D150A, and xanthosine 5′-monophosphate (XMP), pyrophosphate (PP_i), and two Mg^{2+} ions. This structure provides the first view of HGPRT bound to both natural reaction products, complementing recent structures of the 9-deaza-8-azahypoxanthine (HPP)−α-D-5-phosphoribosyl 1-pyrophosphate (PRPP) *Trypanosoma cruzi* HGPRT ternary complex ($HGPRT_{HPP-PRPP-Mg}$; *2*) and of the (1*S*)-1-(9-deazaguanin-9-yl)-1,4-dideoxy-1,4-imino-D-ribitol 5-phosphate (ImmucillinGP)−pyrophosphate human HGPRT ternary complex ($HGPRT_{ImmGP-PP_i-Mg}$; *3*).

Two mechanisms by which HGPRT catalyzes the reaction of purine bases and PRPP to form purine nucleotides have been proposed. In the S_N1-type mechanism, the enzyme promotes the dissociation of pyrophosphate from PRPP, forming an oxocarbenium ion at the ribose $C^{1'}$ atom. It has been proposed that a large, flexible loop (loop II), which

† This work was supported by NIH Grant AI39952 (D.W.B.).

‡ The atomic coordinates and observed structure factors for the XMP−pyrophosphate−Mg^{2+} ternary complex have been deposited in the Protein Data Bank with accession numbers 1qk5 and r1qk5sf, respectively. The atomic coordinates and observed structure factors for the GMP and IMP complexes (see ref *1*) have accession numbers 1qk3, r1qk3sf, 1qk4, and r1qk4sf, respectively.

* To whom correspondence should be addressed: Department of Organic Chemistry, Southern Research Institute, 2000 Ninth Ave. S., Birmingham, AL 35205. E-mail: borhani@sri.org. Phone: (205) 581-2555. Fax: (205) 581-2877.

§ Present address: IntegriDerm, LLC, 2130 Memorial Parkway, SW, Huntsville, AL 35801.

[1] Abbreviations: D150A, *T. gondii* HGPRT Asp150Ala mutant; E, enzyme (HGPRT); GMP, guanosine 5′-monophosphate; Gua, guanine; HGPRT, hypoxanthine-guanine phosphoribosyltransferase; $HGPRT_{Apo}$, *T. gondii* HGPRT−apoenzyme structure; $HGPRT_{dzG-PRPP-Mg}$, *T. gondii* HGPRT−9-deazaguanine−PRPP−Mg^{2+} complex structure; $HGPRT_{GMP}$, *T. gondii* HGPRT−GMP complex structure; $HGPRT_{HPP-PRPP-Mg}$, *T. cruzi* HGPRT−HPP−PRPP−Mg^{2+} complex structure; $HGPRT_{ImmGP-PP_i-Mg}$, human HGPRT−ImmucillinGP−pyrophosphate−Mg^{2+} complex structure; $HGPRT_{IMP}$, *T. gondii* HGPRT−IMP complex structure; $HGPRT_{XMP-PP_i-Mg}$, *T. gondii* HGPRT−XMP−pyrophosphate−Mg^{2+} complex structure; HPP, 9-deaza-8-azahypoxanthine; Hx, hypoxanthine; ImmucillinGP, (1*S*)-1-(9-deazaguanin-9-yl)-1,4-dideoxy-1,4-imino-D-ribitol 5-phosphate; IMP, inosine 5′-monophosphate; NMP, nucleoside 5′-monophosphate; PRPCP, α-D-5-phosphoribosyl 1-(β-methylene)pyrophosphate; PEG, polyethylene glycol; PP_i, pyrophosphate; PRPP, α-D-5-phosphoribosyl 1-pyrophosphate; PRTase, phosphoribosyltransferase; QPRT, quinolinic acid phosphoribosyltranferase; $QPRT_{Phth-PRPCP-Mn}$, *Mycobacterium tuberculosis* QPRT−phthalic acid−PRPCP−Mn^{2+} complex structure; Xan, xanthine; XGPRT, xanthine-guanine phosphoribosyltransferase; XMP, xanthosine 5′-monophosphate.

10.1021/bi990508i CCC: $18.00
Published on Web 10/15/1999

contains an absolutely conserved Ser-Tyr dipeptide, closes over the active site to shield the highly reactive oxocarbenium ion intermediate from nonproductive attack by bulk solvent water molecules. In the S_N2-type mechanism, the enzyme facilitates the simultaneous attack of the purine N^9 atom on, and the departure of pyrophosphate from, ribose $C^{1'}$. Our HGPRT ternary complex structure sheds new light on this mechanistic question.

We describe here how *T. gondii* HGPRT uses Mg^{2+} to orient and activate the pyrophosphate group for catalysis, and we present a comparison of this structure with the structures of three other PRTase ternary complexes (*2*−*4*). Next, we discuss our observation that a critical active site peptide bond can adopt either the cis or the trans configuration. We propose a key role for this isomerization in the energetics of the binding of PRPP and release of pyrophosphate by HGPRT. Finally, we postulate a comprehensive mechanism for HGPRT catalysis. Our mechanism is a synthesis of results from our three *T. gondii* HGPRT crystal structures (*1*), the structures of the *T. gondii* HGPRT apoenzyme (*5*), human HGPRT (*3*, *6*, *7*), *T. cruzi* HGPRT (*2*), and previous detailed kinetic studies (*7*) of human HGPRT.

EXPERIMENTAL PROCEDURES

HGPRT D150A Mutant Construction, Expression, and Purification. T. gondii HGPRT in which Asp150 was mutated to alanine (D150A) was prepared from the wild-type plasmid pETC1 (derivative of pET15b; *8*) with the QuikChange site-directed mutagenesis kit (Stratagene). Polymerase chain reaction (PCR) amplification with *Pfu* DNA polymerase, using plus-strand primer 5′-GTTGAGGACATCGTCGCCACCGGTTTCACCCTC-3′ and minus-strand primer 5′-GAGGGTGAAACCGGTGGCGACGATGTCCTCAAC-3′, was followed by *Dpn*I digestion to remove parental template DNA. Competent *Escherichia coli* XL1-Blue cells were transformed with the PCR product. Screening of ampicillin-resistant colonies by automated DNA sequencing (PRISM Dye Terminator kit/PRISM 377 sequencer, Applied Biosystems, Inc.) confirmed that only the desired mutation had been made. Wild-type human HGPRT (*9*) was cloned into the pET15b vector in a similar manner. Transformation of *E. coli* BL21(DE3) with both plasmids, expression, purification, HGPRT activity assay, and other miscellaneous methods were performed as described for wild-type *T. gondii* HGPRT (*1*).

The kinetics of human HGPRT and *T. gondii* HGPRT were measured spectrophotometrically at 37 °C as described (*1*), in a buffer containing the purine base, PRPP, 100 mM Tris-HCl (pH 8.0), 20 mM $MgCl_2$, 0.1 mM ethylenediaminetetraacetic acid, and 0.1 mg/mL bovine serum albumin. It was experimentally determined that the concentrations of the fixed substrates were saturating (at least 10 times the K_M). K_M and V_{max} values were determined by a nonlinear regression fit to Michaelis−Menten kinetics using ENZFITTER (version 1.05). These fits provided standard errors of less than 17% for the K_M values and less than 10% for the V_{max} values. V_{max} values were converted to k_{cat} values using protein concentrations determined by the Bradford assay (*10*), using bovine γ globulin as the standard. These concentrations agreed well with those determined spectrophotometrically, using calculated extinction coefficients (*11*).

Table 1: Kinetic Parameters for Nucleotide Formation by *T. gondii* and Human HGPRT[a]

HPRT Reaction					
		K_M (μM)		k_{cat}/K_M (μM^{-1} s^{-1})	
enzyme	k_{cat} (s^{-1})	Hx	PRPP	Hx	PRPP
T. gondii WT	7.59	1.6 ± 0.6	42.9 ± 4.2	4.63	0.177
T. gondii D150A	0.69	2.3	7.4	0.296	0.093
human	15.7	2.4	15.2	6.48	1.03
GPRT Reaction					
		K_M (μM)		k_{cat}/K_M (μM^{-1} s^{-1})	
enzyme	k_{cat} (s^{-1})	Gua	PRPP	Gua	PRPP
T. gondii WT	12.7	2.1 ± 0.7	74.6 ± 20.0	6.02	0.170
T. gondii D150A	0.04	2.4	12.1	0.018	0.004
human	70.3	4.2	32.8	16.8	2.14
XPRT Reaction					
		K_M (μM)		k_{cat}/K_M (μM^{-1} s^{-1})	
enzyme	k_{cat} (s^{-1})	Xan	PRPP	Xan	PRPP
T. gondii WT	31.0	14.4 ± 1.7	146 ± 35	2.15	0.213
T. gondii D150A	3.61	47.2	19.9	0.076	0.181
human	0.27	20.0	237	0.013	0.001

[a] Kinetic parameters were determined at pH 8.0 and 37 °C. The errors reported for the wild-type (WT) *T. gondii* HGPRT Michaelis constants are standard deviations (five different enzyme preparations).

Crystallization and Data Collection. T. gondii HGPRT (D150A mutant, 10−20 mg/mL) containing 1 mM PRPP, 1 mM xanthine, and 10 mM $MgCl_2$ was mixed with an equal volume of the precipitant [30% polyethylene glycol (PEG) 4000, 100 mM Tris-HCl, and 200 mM Li_2SO_4 (pH 8.5)] and equilibrated against the precipitant at 4 °C (hanging drops). Thin, plate-like crystals (space group $C222_1$, a = 55.21 Å, b = 112.25 Å, and c = 144.24 Å) grew in about 2 days. A crystal was harvested into mother liquors containing 40% PEG 4000 and up to 30% glycerol as the cryoprotectant, and was then flash-cooled in liquid nitrogen. X-ray diffraction data were collected at the National Synchrotron Light Source (beamline X25, λ = 1.100 Å, Brandeis B4 CCD detector) by the rotation method (0.5−1.0°, exposure for 30−120 s) at 100 K. Data processing was performed as described in ref *1*. The diffraction data are summarized in Table 2.

Structure Determination. The self-rotation function (AMORE) (*12*) revealed the presence of two HGPRT subunits in the $C222_1$ asymmetric unit. They are transformed into the complete HGPRT tetramer by application of a crystallographic 2-fold rotation parallel to the *b* axis. The structure was determined by molecular replacement (AMORE), using the structure of the HGPRT−GMP complex (subunit A) as the search model (*1*). The complete tetramer was placed in the unit cell in a position consistent with the cross-rotation and translation functions. Rigid-body fitting of the appropriate two subunits in the asymmetric unit gave a correlation coefficient of 16% (13−3 Å). Refinement of these two subunits with X-PLOR (*13*) [with torsion angle molecular dynamics (*14*), noncrystallographic symmetry constraints, and then restraints] and model building (O) (*15*) lowered R_{free} to 34.3% (10−1.6 Å). $2F_o - F_c$ and $F_o - F_c$ maps showed clear electron density in the active site for a cis peptide bond between residues Leu78 and Lys79, XMP, and pyrophos-

Table 2: Data Collection and Refinement Statistics

	D150A mutant
Crystal Parameters	
ligands	XMP, pyrophosphate, Mg^{2+}
space group	$C222_1$
a (Å)	55.21
b (Å)	112.25
c (Å)	144.28
volume (Å^3)	894150
no. of subunits per asymmetric unit	2
Data Collection Statistics	
resolution range (Å)	13.0−1.60
no. of observations	245248
no. of unique reflections	58200
mosaicity (deg)	0.5
overall	
R_{sym} (%)	7.6
I/σ_I	10.3
data completeness (%)	98.0
mean multiplicity	4.2
highest-shell	
resolution range (Å)	1.60−1.66
R_{sym} (%)	37.3
I/σ_I	2.4
data completeness (%)	93.9
mean multiplicity	3.7
Refinement Statistics	
no. of reflections used in R_{cryst} ($F > 0\sigma_F$)	55139
no. of reflections used in R_{free} ($F > 0\sigma_F$)	2953
R_{cryst} (%)	23.4
R_{free} (%)	26.1
rmsd for bond lengths (Å)	0.015
rmsd for bond angles (deg)	2.3
Ramachandran plot (% allowed, generously allowed, and disallowed residues)	99.7, 0.3, 0
no. of atoms [protein (including alternate conformations), ligands, water]	3472, 70, 182
average *B*-factors (Å^2) (protein, ligand, water)	24.8, 27.9, 29.1

phate coordinated to two Mg^{2+} ions, each with a complement of water molecules. Refinement was completed with several rounds of refinement with REFMAC (*16*) and ARP (*17*), with unrestrained Mg^{2+} ions. The refinement is summarized in Table 2. The final model consists of 434 out of 460 possible amino acids, two XMP molecules, two pyrophosphate ions, four Mg^{2+} ions, and 182 water molecules. Residues in loop II (residues 117−127 in subunit A and 117−125 in subunit B) and loop III′ (residues 181−184) were not located. The quality of the model was checked with PROCHECK (*18*), WHATIF (*19*), and WHATCHECK (*20*). The figures were prepared with RIBBONS (*21*).

RESULTS AND DISCUSSION

We have determined the crystal structures of *T. gondii* HGPRT in the presence of its three natural reaction products, the nucleotides GMP, IMP, and XMP. In the preceding article (*1*), the structures of the GMP and IMP complexes are described, and the structural basis for the differential binding of purine bases by human and *T. gondii* HGPRT is discussed. Here, we report on the unique structural features of the XMP complex, which also contains pyrophosphate and two Mg^{2+} ions. We refer to these three structures as $HGPRT_{GMP}$, $HGPRT_{IMP}$, and $HGPRT_{XMP-PP_i-Mg}$, respectively. The structure of the *T. gondii* HGPRT apoenzyme, determined previously by Schumacher et al., will be called $HGPRT_{Apo}$ (*5*).

Properties and Steady-State Kinetic Parameters of D150A

A mutant form of *T. gondii* HGPRT was prepared in which the active site base (*6*), Asp150, was replaced with alanine (D150A). The mutant enzyme was purified to apparent homogeneity by the procedures used for wild-type *T. gondii* HGPRT (*1*). Gel filtration of D150A showed that it was a tetramer, like the wild-type enzyme. The enzymatic activity of D150A was stable to storage at −20 °C in 50% glycerol. The steady-state kinetic parameters for both wild-type and D150A *T. gondii* HGPRT were measured at pH 8.0 and 37 °C. These results are presented in Table 1, as are the parameters for human HGPRT.

T. gondii HGPRT D150A had significantly decreased enzymatic activity compared to the wild-type enzyme. This was due predominantly to decreases in k_{cat}, which was reduced 11-, 296-, and 8.6-fold with hypoxanthine, guanine, and xanthine as substrates, respectively (Table 1). Further kinetics experiments to determine why k_{cat} for guanine is so low compared to k_{cat} for hypoxanthine and xanthine are underway. A similar effect was noticed with the analogous human HGPRT D137N mutant (*7*). Like human HGPRT D137N, *T. gondii* HGPRT D150A exhibited little change in the Michaelis constants for the purine bases, whereas the K_M values for PRPP were reduced ∼6-fold.

Crystal Structure of T. gondii HGPRT D150A

The D150A mutant of *T. gondii* HGPRT was crystallized, in the presence of xanthine, PRPP, and $MgCl_2$, under conditions that provided crystals of the IMP complex in space group $P2_12_12_1$ (*1*). Catalysis occurred during crystallization, yielding a complex of HGPRT D150A, XMP, pyrophosphate, and two Mg^{2+} ions in space group $C222_1$. The structure was determined by molecular replacement and refined at 1.60 Å resolution (Table 2). The substitution of alanine for Asp150 was confirmed (Figure 1). Unlike the $HGPRT_{GMP}$ and $HGPRT_{IMP}$ structures (*1*), the crystallographic asymmetric unit of $HGPRT_{XMP-PP_i-Mg}$ consisted of only two HGPRT subunits. Application of a crystallographic 2-fold rotation to these two subunits, however, generated the complete HGPRT tetramer. The tertiary and quaternary structures of $HGPRT_{XMP-PP_i-Mg}$ are generally very similar to the other two structures. Details about how *T. gondii* HGPRT binds the xanthine moiety of XMP compared to guanine and hypoxanthine of GMP and IMP are presented in the preceding article (*1*). Here, we focus on the binding of pyrophosphate and Mg^{2+} by the enzyme.

Catalytic Role of Mg^{2+}—Binding of Pyrophosphate

The structure of $HGPRT_{XMP-PP_i-Mg}$ shows for the first time how HGPRT binds the reaction products XMP and pyrophosphate, as well as how Mg^{2+} binds and orients the pyrophosphate group for catalysis. As shown in Figure 2, the pyrophosphate is firmly bound between active site loops I (Leu78−Gly83) and IV (Gly202−His216), and is connected to both loops and the core and hood domains by an extensive network of hydrogen bonds and two Mg^{2+} ion-

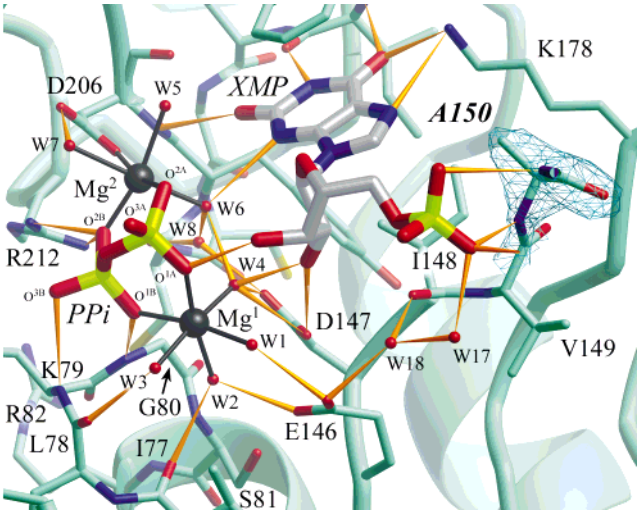

FIGURE 1: *T. gondii* $HGPRT_{XMP-PP_i-Mg}$ active site. The protein (subunit B) is shown in a RIBBONS (*21*) representation (green). XMP and pyrophosphate are colored by atom type (carbon, silver; nitrogen, blue; oxygen, red; and phosphorus, yellow-green). Water molecules and the two Mg^{2+} ions are represented by red and black spheres, respectively, and hydrogen bonds are shown as gold cones. The hood and core domains are at the upper back and lower front, respectively. The simulated annealing omit map electron density for Ala150 (site of the D150A mutation), shown as a blue net ($2F_o - F_c$, 1σ), clearly shows that the carboxylate side chain is not present. Note the water-mediated coordination of Mg^1 compared to the direct coordination of Mg^2 by Asp206. Pyrophosphate O^{3B} is hydrogen bonded to the NH of the cis peptide bond between Leu78 and Lys79 in loop I.

mediated coordination spheres. [The secondary structure of *T. gondii* HGPRT is shown in Figure 1 of the preceding article (*1*), and Figure 2 shows a sequence alignment of human and protozoal HGPRTs (*1*).] Each Mg^{2+} ion has octahedral coordination involving two terminal oxygen atoms of the pyrophosphate, which adopt a cis orientation around the Mg^{2+}, and four (Mg^1) or three (Mg^2) water molecules (Table 3). Mg^2 is also coordinated by the side chain carboxylate of the absolutely conserved aspartic acid, Asp206. This is the only direct contact between HGPRT and the Mg^{2+} ions. The neurological disorder Lesch-Nyhan syndrome (*22*) is caused by various mutations in human HGPRT (*23*), among them mutation of homologous Asp193 to asparagine ($HGPRT_{Kinston}$), which dramatically alters the kinetic parameters compared to those of wild-type HGPRT (K_M for hypoxanthine and PRPP elevated 160- and 125-fold, respectively; *24*). The two Mg^{2+} ions impose an eclipsed conformation upon the oxygen atoms of pyrophosphate. This configuration is common in structures where pyrophosphate is coordinated to either one or two divalent metal ions. The two Mg^{2+} ions are separated by 4.8 and 4.9 Å in the A and B subunits, respectively. They share no ligands other than the pyrophosphate. The equatorial planes of the two Mg^{2+} ion coordination spheres (defined below) intersect at angles of 118° (A) and 110° (B), thereby causing the axial direction of the coordination spheres to converge behind and under the ribose ring. The coordination spheres in subunits A and B differ slightly (Table 3).

There is very clear electron density for XMP, pyrophosphate, two Mg^{2+} ions, and their surrounding water molecules (Figure 2). The average temperature factors for the pyrophosphate ions, the Mg^{2+} ions, and their coordinating water

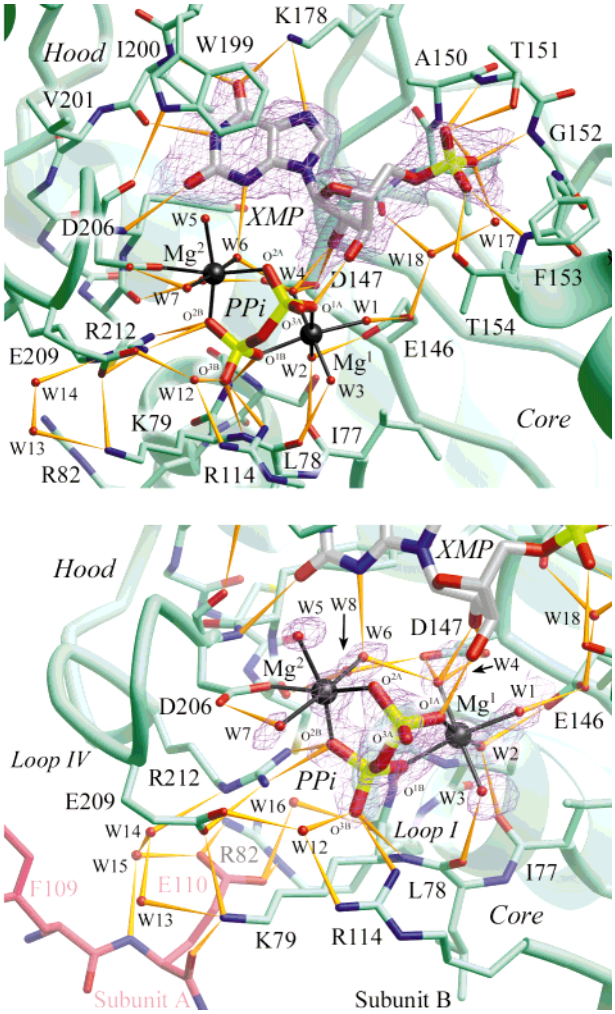

FIGURE 2: Binding interactions of XMP, Mg^{2+}, and pyrophosphate in the *T. gondii* $HGPRT_{XMP-PP_i-Mg}$ active site. (Top) The upper active site. This view is approximately perpendicular to the view shown in Figure 1. Simulated annealing omit map electron density for XMP is shown as a lavender net. Note the extensive hydrogen bonding network that links the protein, the pyrophosphate, the Mg^{2+} ions, and the ordered water molecules. This view also shows how pyrophosphate oxygen atom O^{1A} (directly above Mg^1) is oriented for attack on the C1′ atom of XMP. Also apparent are the extensive links between loop I (bottom) and loop IV (left), mediated in part by the distal pyrophosphate oxygen atoms. (Bottom) The lower active site. Subunit B is shown in green, and subunit A is shown in rose. Simulated annealing omit map electron density for the pyrophosphate ion, the two Mg^{2+} ions, and their coordinating water molecules is shown as a lavender net. The active site of subunit A, ~20 Å distant from the subunit B active site shown here, is located off the picture, below the Subunit B label.

molecules are 22.8, 27.7, and 29.2 $Å^2$, respectively, which are comparable to those of the surrounding protein residues in the active site. Accordingly, we believe that these ligands are present in the active site of $HGPRT_{XMP-PP_i-Mg}$ at full occupancy.

Mg^{2+} Coordination Geometry. Mg^1 is nestled between the C-terminal end of the core domain β-sheet, active site loops II (Arg114−Leu134) and III (Asp150−Thr154), and the α-face of the ribose ring. It is not coordinated by HGPRT directly, but rather through water-mediated hydrogen bonds (Figures 1 and 2; interactions are summarized in Figure 3 and Table 3). The pyrophosphate oxygen atoms O^{1A} and O^{1B} and waters Wat1 and Wat2 define the equatorial plane of

Table 3: Mg^{2+}, Pyrophosphate, and Water Interactions in the Active Site

ligand	atom 1	atom 2	interatomic distance (Å) subunit A	subunit B
M1	Mg^1	PP_i O^{1A}	2.06	2.09
		PP_i O^{1B}	2.09	2.24
		Wat1	2.16	2.24
		Wat2	2.26	2.25
		Wat3	2.38	2.14
		Wat4	−	2.08
	Wat1	Glu146 $O^{\epsilon 1}$	2.58	2.78
		XMP $O^{2'}$	2.53	3.42
		XMP $O^{3'}$	2.64	3.23
	Wat2	Ile77 O	3.14	2.90
		Glu146 $O^{\epsilon 2}$	2.72	2.73
	Wat3	Leu78 O	3.00	2.77
		Leu115 O	2.64	2.63
	Wat4	Asp147 $O^{\delta 1}$	−	2.91
		Asp147 $O^{\delta 2}$	−	2.61
		XMP $O^{2'}$	−	2.47
		Wat6	−	2.70
M2	Mg^2	Asp206 $O^{\delta 1}$	2.13	2.25
		PP_i O^{2A}	2.36	2.31
		PP_i O^{2B}	2.09	2.00
		Wat5	2.23	2.30
		Wat6	2.16	2.29
		Wat7	2.02	2.40
	Wat5	Wat9	2.74	−
	Wat6	XMP O^2	3.20	3.50
		XMP N^3	2.98	3.04
		Wat8	2.65	2.58
	Wat7	Asp206 $O^{\delta 2}$	2.67	2.57
	Wat8	Asp147 $O^{\delta 2}$	2.78	2.66
		Cys204 O	2.74	2.86
	Wat9	Asn208 N	3.01	−
pyrophosphate	O^{1A}	XMP $C^{1'}$	4.37	4.44
		XMP $O^{3'}$	2.54	2.46
		Wat10	2.93	3.03
	O^{1B}	Gly80 N	2.70	2.67
	O^{2B}	Arg212 $N^{\eta 1}$	3.18	3.06
		Arg212 $N^{\eta 2}$	2.87	2.77
	O^{3A}	Wat11	2.74	−
	O^{3B}	Lys79 N	2.92	3.08
		Arg114 $N^{\eta 1}$	2.86	2.93
		Wat12	2.70	2.58
HGPRT lower active site	Lys79 O	Wat16	2.91	2.87
	Lys79 N^{ζ}	Glu110 O^a	3.02	3.04
		Glu209 $O^{\epsilon 1}$	3.19	3.02
		Wat13	3.16	3.05
	Arg82 N^{ϵ}	Glu110 $O^{\epsilon 2}$ [a]	3.06	3.04
	Arg82 $N^{\eta 1}$	Glu110 $O^{\epsilon 1}$ [a]	2.96	3.03
	Glu110 N^a	Wat15	2.96	2.94
	Glu110 O^a	Wat13	2.85	2.85
		Wat16	2.70	2.90
	Arg114 $N^{\eta 2}$	Wat12	2.86	2.93
	Cys204 O	Arg212 $N^{\eta 1}$	2.87	2.99
	Asp206 $O^{\delta 1}$	Arg212 $N^{\eta 1}$	3.25	3.27
	Glu209 O	Wat14	2.92	2.91
	Glu209 $O^{\epsilon 1}$	Arg212 $N^{\eta 2}$	2.91	2.90
	Glu209 $O^{\epsilon 2}$	Wat12	2.65	2.76
	Arg212 N^{ϵ}	Wat14	3.01	2.92
	Wat13	Wat14	2.75	2.74
	Wat14	Wat15	2.69	2.74

[a] Glu110 of the other subunit.

Mg^1. Wat1, trans to the distal pyrophosphate oxygen O^{1B}, is hydrogen bonded to the carboxylate side chain of invariant residue Glu146 (syn lone pair of $O^{\epsilon 1}$). [The pyrophosphate ion atoms are named such that the "A" phosphate group (atoms P^A, O^{1A}, O^{2A}, and O^{3A}) is proximal to the nucleotide, whereas the "B" phosphate (P^B, etc.) is distal.] Wat2, trans to the proximal pyrophosphate oxygen O^{1A}, is hydrogen bonded to the carbonyl oxygen of Ile77 and the anti lone pair of Glu146 $O^{\epsilon 2}$. Axial ligand Wat3, which projects outward from the active site toward the solvent, is hydrogen bonded to pyrophosphate oxygens O^{1A} and O^{1B}, as well as to the carbonyl oxygen of Leu78 (part of the cis peptide bond; see below). The other axial ligand Wat4 (subunit B only) points inward and is hydrogen bonded to Wat6 (an axial ligand of Mg^2), the carboxylate side chain of invariant Asp147 (syn lone pairs of both $O^{\delta 1}$ and $O^{\delta 2}$), and ribose $O^{2'}$. The Wat4−Wat6 hydrogen bond is the only link between the two Mg^{2+} coordination spheres other than the pyrophosphate itself.

Mg^2 is located at the cleft between the core and hood domains, adjacent to the purine ring (Figure 2; summarized in Figure 3 and Table 3). Two pyrophosphate oxygen atoms (O^{2A} and O^{2B}), Wat5, and $O^{\delta 1}$ (syn lone pair) of the invariant residue Asp206 define the equatorial ligand plane, with $O^{\delta 1}$ trans to the proximal pyrophosphate oxygen O^{2A}. Wat5 is in van der Waals contact with Trp199 $C^{\zeta 2}$. The axial ligand Wat6, located deep in the active site, is hydrogen bonded to xanthine O^2 and N^3, pyrophosphate O^{2A}, and Wat8, which is in turn hydrogen bonded to the carbonyl oxygen atom of Cys204 and $O^{\delta 2}$ of Asp147. The other axial ligand Wat7 projects out of the active site and is hydrogen bonded to $O^{\delta 2}$ of Asp206.

Additional Pyrophosphate Interactions. The distal pyrophosphate oxygen atoms (O^{1B}, O^{2B}, and O^{3B}), at the bottom of the active site cleft, are the cornerstone upon which an extensive hydrogen bond network is built (Figures 2 and 3 and Table 3). This network links the core domain to the hood domain, and serves as a bridge of communication between active sites within the HGPRT tetramer. O^{1B} and O^{3B} are hydrogen bonded to the peptide NHs of Gly80 and Lys79 (cis peptide bond), respectively. Pyrophosphate oxygen O^{2B} is hydrogen bonded to both terminal nitrogen atoms of Arg212; the $N^{\eta 1}$ atom of this residue is in turn linked to the carbonyl oxygen of Cys204 and $O^{\delta 1}$ (the Mg^2 ligand) of Asp206. O^{3B} is also hydrogen bonded to the $N^{\eta 1}$ atom of Arg114 and to Wat12, which is linked to $N^{\eta 2}$ of Arg114 and $O^{\epsilon 2}$ of Glu209. The network wraps around the pyrophosphate as Glu209 $O^{\epsilon 1}$ is connected to Arg212 $N^{\eta 2}$ as well. Extending outward toward the adjacent subunit in the HGPRT tetramer, a large number of direct and water-mediated (Wat13, Wat14, Wat15, and Wat16) hydrogen bonds link residues Lys79, Arg82, Glu209, and Arg212 in subunit B with residue Glu110 in subunit A (Table 3). Glu110 is itself linked to a further spine of hydration along the subunit A−subunit B interface that extends to the active site of subunit A.

Two mutations in the lower active site make human HGPRT a cooperative enzyme [$HGPRT_{MooseJaw}$ (gouty arthritis phenotype), Asp193Glu, Hill coefficient = 2.3 (*25*), and Lys68Ala, Hill coefficient ~ 1.9 (*26*)]. To date, the only structural element by which the cooperativity of these mutants can be understood is the extensive hydrogen bond network that links these residues in one active site to the active site of the adjacent subunit in the HGPRT tetramer (Figure 2, bottom). These mutations should alter both the positions of Mg^2 and pyrophosphate and the hydrogen bond network that connects subunit A to subunit B. Thus, in the mutants, when PRPP is bound to subunit A, the active site of subunit B is affected.

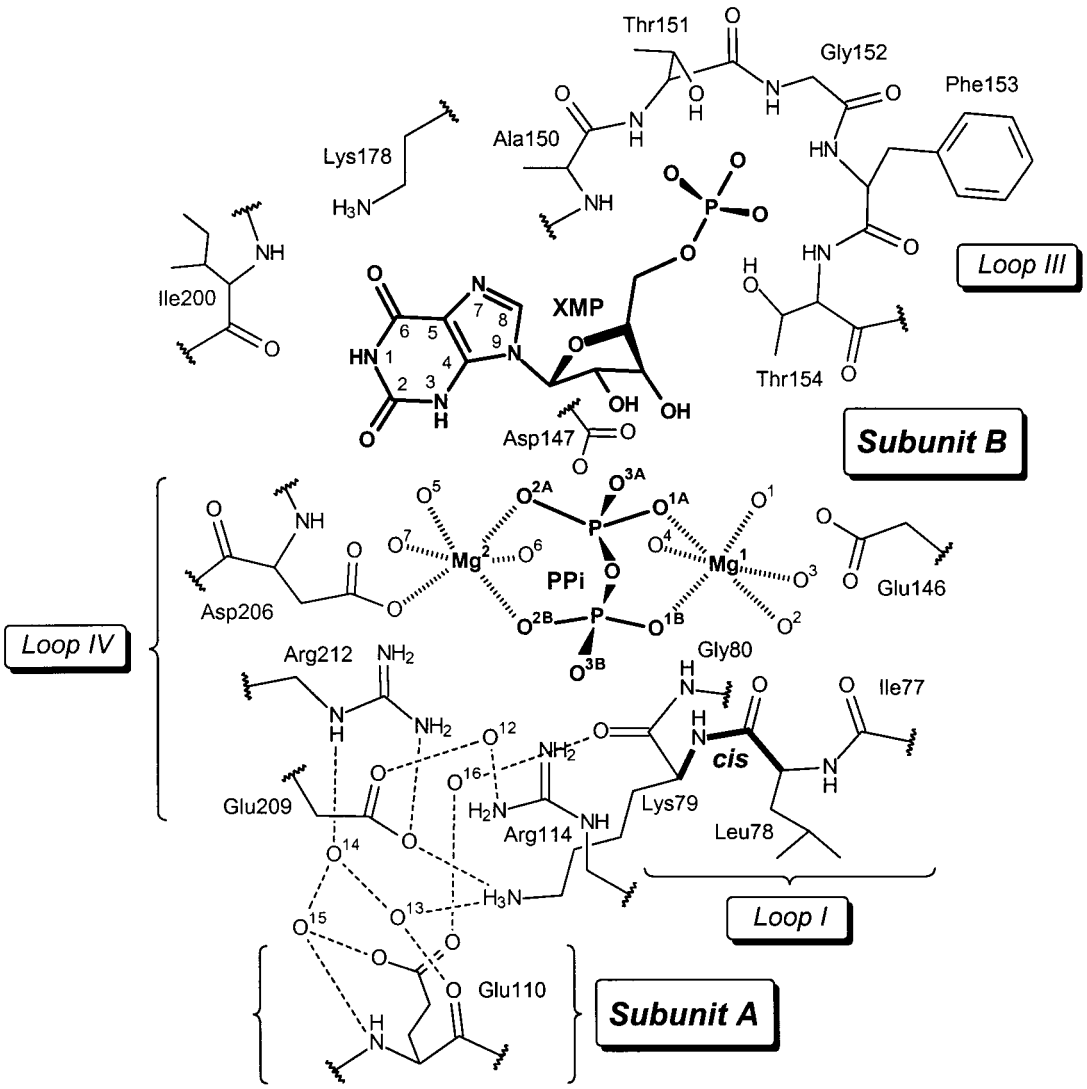

FIGURE 3: Schematic representation of the active site. Most of the hydrogen bonds between HGPRT and the ligands (bold) are omitted for clarity (see Table 3). Hydrogen bonds that link loops I and IV in the lower active site, and that link the active sites of subunits A and B, are shown as dotted lines.

Additional XMP Interactions. As was described for the GMP and IMP complexes in the preceding article (*1*), the 5′-phosphate group of XMP is located in a tight cradle formed by loop III. The hydrogen bonding pattern is essentially identical to that described for GMP and IMP, with one addition. O^{2P} is hydrogen bonded through a bridging water, Wat17, to the peptide NH of Leu155. Wat17 is hydrogen bonded to Wat18, itself hydrogen bonded to $O^{\epsilon 1}$ (anti lone pair) of Glu146 and the carbonyl oxygen of Ile148. These two water molecules therefore link the hydrogen bonding network of the phosphate group with that of Mg^{2+}–pyrophosphate.

Geometry and Nature of Catalysis

In the $HGPRT_{XMP-PP_i-Mg}$ structure, the XMP ribose $C^{1'}$ is 4.4 Å away from the pyrophosphate oxygen atom, O^{1A}, best oriented for nucleophilic attack (Figures 1 and 2). The angle between xanthine N^9, ribose $C^{1'}$, and pyrophosphate O^{1A} is 160°, close to the optimal 180° required for S_N2 backside displacement. Oxygen O^{2A} is slightly closer to $C^{1'}$ (4.2 and 4.0 Å in subunits A and B, respectively), but it is not oriented well (129° and 134° in subunits A and B, respectively). It is interesting to note that O^{1A} is a Mg^1 ligand. From the point of view of the reverse reaction (XMP pyrophosphorolysis), it would seem that the unliganded proximal oxygen, O^{3A}, which is located 5.7 Å from $C^{1'}$, would be a better nucleophile, in that its electron density is not donated to a Mg^{2+} ion. In the forward reaction (XMP synthesis), O^{1A} would clearly be the better leaving group, however, since its charge would be distributed onto the Mg^{2+} ion. By the principle of microscopic reversibility, the nucleophile in the reverse reaction must be one and the same with the leaving group in the forward reaction. We suggest therefore that this attacking atom is O^{1A}. The two Mg^{2+} ions bound at the HGPRT active site therefore play two roles. They increase the leaving group propensity of the pyrophosphate moiety of PRPP, and they enforce upon this group the optimal geometry for departure.

There has been much discussion in the literature on how the large active site loop II closes during catalysis to shield reactive intermediates in the active site from bulk solvent. Our $HGPRT_{XMP-PP_i-Mg}$ structure shows that when loop II is *open*, 10 water molecules are present in the active site in proximity to the $C^{1'}$ atom of PRPP. When loop II is *closed*,

however, these same water molecules are still present, trapped inside the active site [structures of *T. cruzi* $HGPRT_{HPP-PRPP-Mg}$ (*2*), human $HGPRT_{ImmGP-PP_i-Mg}$ (*3*), and *T. gondii* HGPRT with 9-deazaguanine, PRPP, and two Mg^{2+} ions bound at 1.05 Å resolution ($HGPRT_{dzG-PRPP-Mg}$) (*27*)]. Since closure of loop II does not exclude or expel water from the HGPRT active site, and since there is no mechanistic rationale for shielding an active site already filled to capacity with water from bulk solvent, we conclude that closure of loop II serves another purpose, namely, the final enforcement of propinquity that drives the substrates to the transition state.

Furthermore, it has been debated whether HGPRT operates by a dissociative S_N1 mechanism or by an associative S_N2 mechanism. Yet, discussion of whether the *character* of the active site is appropriate for the obligatory S_N1 intermediate, an oxocarbenium ion, has been missing from this debate. Were the reaction to proceed by an S_N1 mechanism in the closed, highly hydrated HGPRT active site, significant nonproductive quenching of the oxocarbenium ion intermediate by the trapped water might be expected to occur. The fact that this does not happen suggests that the reaction proceeds rather by an S_N2 mechanism. The relative geometry of the products in the $HGPRT_{XMP-PP_i-Mg}$ structure is consistent with such a mechanism. And, the ~1000-fold enhancement of binding of ImmucillinGP by HGPRT (*28*), compared to that by GMP or carbocyclic GMP, is also consistent with an S_N2 mechanism, which in the transition state would have a partial positive charge at $C^{1'}$ resonance-stabilized by the lone pair electrons of O^4.

Comparison of Pyrophosphate Ligation in Four PRTases

Comparison of three recently determined PRTase ternary complex structures [*T. cruzi* $HGPRT_{HPP-PRPP-Mg}$ (*2*), human $HGPRT_{ImmGP-PP_i-Mg}$ (*3*), and *Mycobacterium tuberculosis* quinolinic acid phosphoribosyltranferase (QPRT) with substrate analogues phthalic acid and 5-phosphoribosyl 1-(β-methylene)pyrophosphate (PRPCP) and two Mn^{2+} ions bound ($QPRT_{Phth-PRPCP-Mn}$) (*4*)] with that of *T. gondii* $HGPRT_{XMP-PP_i-Mg}$ suggests that the location of the pyrophosphate moiety and the two metal ions, and the coordination sphere of these ions, is similar in all four structures. In particular, in *T. cruzi* $HGPRT_{HPP-PRPP-Mg}$ and human $HGPRT_{ImmGP-PP_i-Mg}$, the two metal ions are coordinated by only one protein ligand (Asp171 and Asp193, respectively), which corresponds to Asp206 in *T. gondii* HGPRT. Despite the completely different protein fold of the type II QPRT and the type I HGPRTs, a similar arrangement is seen in this case as well.

Nonetheless, there are differences in how the three HGPRTs bind metal ions and pyrophosphate. These differences likely arise because these three structures represent different points along the HGPRT reaction coordinate. The octahedral coordination of M1 (Mn^{2+}; see below) in *T. cruzi* $HGPRT_{HPP-PRPP-Mg}$ is distorted, with the PRPP ribose $O^{2'}$ and $O^{3'}$ atoms taking the place of waters Wat4 and Wat1 around the metal ion (*2*). Also, a weak (2.6 Å) interaction between M1 and the PRPP O^1 oxygen atom, which connects the ribose ring to the pyrophosphate, replaces the strong interaction (2.1 Å) between the proximal pyrophosphate oxygen O^{1A} and Mg^1 in *T. gondii* $HGPRT_{XMP-PP_i-Mg}$. The Mg^{2+}−pyrophosphate structure in human $HGPRT_{ImmGP-PP_i-Mg}$ resembles that found in $HGPRT_{HPP-PRPP-Mg}$, with a weak $Mg^{2+}-O^{1A}$ bond (2.4−2.5 Å) and coordination of Mg^{2+} by both ribose hydroxyl groups. The changes in the ligation of M1 are likely responsible in part for the differences in the intermetal distances observed in these structures. In *T. gondii* $HGPRT_{XMP-PP_i-Mg}$, the two metal ions are separated by 4.8 and 4.9 Å, compared to 5.4 and 5.6 Å in *T. cruzi* $HGPRT_{HPP-PRPP-Mg}$ (*2*) and 4.6−5.1 Å in human $HGPRT_{ImmGP-PP_i-Mg}$ (*3*).

The interactions between pyrophosphate and the protein also differ between the three HGPRTs. In *T. cruzi* $HGPRT_{HPP-PRPP-Mg}$ and human $HGPRT_{ImmGP-PP_i-Mg}$, the peptide NHs of the conserved Ser-Tyr dipeptide of (closed) loop II hydrogen bond to the proximal, non-Mg^{2+}-ligated pyrophosphate oxygen atom O^{3A} (*2*, *3*). In *T. cruzi* HGPRT, this interaction between loop II and the pyrophosphate, which has no counterpart in *T. gondii* $HGPRT_{XMP-PP_i-Mg}$, comes at the expense of losing three hydrogen bonds between the distal pyrophosphate oxygen atoms and the cis peptide bond (Leu51−Lys52 in loop I). These latter hydrogen bonds *are* observed in both *T. gondii* $HGPRT_{XMP-PP_i-Mg}$ and the second subunit in the *T. cruzi* $HGPRT_{HPP-PRPP-Mg}$ structure, in which loop II is open, as well as in $HGPRT_{ImmGP-PP_i-Mg}$ and *T. gondii* $HGPRT_{dzG-PRPP-Mg}$ (*27*), in which loop II is closed. Thus, it appears that the detailed interactions between protein and pyrophosphate depend on the position of loop II and the contents of the active site.

In *T. cruzi* HGPRT, the M1 metal ion is Mn^{2+} rather than Mg^{2+}. The Mn^{2+} is apparently a tight-binding contaminant (*2*). In contrast, in both human $HGPRT_{ImmGP-PP_i-Mg}$ (*3*) and *T. gondii* $HGPRT_{XMP-PP_i-Mg}$, there is no evidence (low temperature factors or abnormally strong electron density) of the binding of Mn^{2+} rather than Mg^{2+} at this site. Although *T. gondii* HGPRT is catalytically active in the presence of Mn^{2+} (~20% of the normal activity), unlike that of *T. cruzi* HGPRT, its Mg^{2+}-dependent activity is not enhanced by the addition of Mn^{2+} (E. L. White, L. J. Ross, and D. W. Borhani, unpublished observations).

Comparison of Transition-State Geometry. In *T. gondii* $HGPRT_{XMP-PP_i-Mg}$, the pyrophosphate is ideally situated for catalysis, either as the leaving group of PRPP in the forward reaction or as the nucleophile for XMP pyrophosphorolysis in the reverse reaction. In particular, the angle between the incoming nucleophile and departing leaving group atoms (pyrophosphate O^{1A} and XMP N^9) around the ribose $C^{1'}$ atom is 160°. In *T. cruzi* $HGPRT_{HPP-PRPP-Mg}$, the reactants appear to be similarly oriented, though the angle between HPP C^9, PRPP $C^{1'}$, and PRPP O^1 was not mentioned in this paper (*2*). Also, the closure of loop II in the *T. cruzi* structure likely tightens the geometry of this ternary complex toward the transition state more than in *T. gondii* $HGPRT_{XMP-PP_i-Mg}$, accounting for the observed difference in the $C^9-C^{1'}$ (*T. cruzi*) and $C^{1'}-O^{1A}$ (*T. gondii*) distances (3.8 and 4.4 Å, respectively). In human $HGPRT_{ImmGP-PP_i-Mg}$, this distance is even closer (3.3−3.6 Å), similar to the $C^9-C^{1'}$ distance we observe in the *T. gondii* $HGPRT_{dzG-PRPP-Mg}$ ternary complex (3.5 Å; *27*), and the angle is 166° (*3*).

Two Isomers of a Critical Active Site Peptide Bond

Cis Peptide Bond. There is a cis peptide bond between Leu78 and Lys79 (loop I) in $HGPRT_{XMP-PP_i-Mg}$. The corre-

sponding peptide bond in *T. cruzi* $HGPRT_{HPP-PRPP-Mg}$ is cis as well (*2*). Since non-proline cis peptide bonds are very rare in protein structures, occurring in only 0.05% of the protein peptide bonds (*29*), this cis peptide bond is presumably essential to the catalytic mechanism of HGPRT. Indeed, these and other HGPRT crystal structures support this hypothesis, showing that the cis peptide bond serves three critical functions. First, its peptide NH forms a direct hydrogen bond with the distal pyrophosphate oxygen atom O^{3B}. The geometry of this interaction is very similar to that seen in dihydrofolate reductases, where an absolutely conserved cis Gly-Gly dipeptide at the base of the active site forms a hydrogen bond with the pyrophosphate moiety of the DHFR cofactor, NADPH. Second, the cis peptide bond positions Gly80 to hydrogen bond with pyrophosphate oxygen O^{1B}. Third, the cis peptide bond orients the side chain of Lys79 so that it can participate in the extensive hydrogen bond network at the bottom of the active site cleft and at the subunit A−subunit B interface. Were the peptide bond between Leu78 and Lys79 in the trans configuration, none of these interactions would be possible.

Trans Peptide Bond. It was surprising, therefore, given the critical role of a cis Leu78−Lys79 peptide bond in the binding of PRPP and pyrophosphate at the active site, to find that this peptide bond adopts the trans configuration in *T. gondii* $HGPRT_{GMP}$ (*1*) and $HGPRT_{Apo}$ (*5*), and in the GMP and IMP complexes of human HGPRT (*6*, *7*). The trans geometry causes the main chain of *T. gondii* $HGPRT_{GMP}$ to deviate from the path followed in $HGPRT_{IMP}$ and $HGPRT_{XMP-PP_i-Mg}$ from Lys79 to Phe83 (start of helix E). This geometry also places the side chain of Lys79 in the vicinity of the ribose ring and loop III, in the upper part of the active site, where it makes various interactions. In $HGPRT_{Apo}$, the course of loop I roughly mimics that found in $HGPRT_{IMP}$ and $HGPRT_{XMP-PP_i-Mg}$, despite the presence of the trans peptide bond. A somewhat geometrically distorted Lys79 extends toward the hood domain to interact with Asp209. In human HGPRT−GMP and HGPRT−IMP, loop I adopts yet another path, which places the homologous residue, Lys68, in the space occupied by pyrophosphate in $HGPRT_{XMP-PP_i-Mg}$, where it diverts the Mg^{2+} ligand, $O^{\delta 1}$ of Asp193, into a salt bridge interaction.

Neither PRPP nor pyrophosphate can bind to HGPRT when loop I adopts any of these trans peptide bond-induced altered conformations, due to both a direct steric block (Lys79 occupying the pyrophosphate binding groove) and the loss of hydrogen bonds to the peptide NHs of Lys79 and Gly80, which allow loop I to approach the pyrophosphate closely. Our *T. gondii* $HGPRT_{XMP-PP_i-Mg}$ structure and that of *T. cruzi* $HGPRT_{HPP-PRPP-Mg}$ indicate that this peptide bond must adopt the cis configuration to allow PRPP binding. Although this peptide bond is trans in both human HGPRT nucleotide complex crystal structures reported to date, it must also adopt the cis configuration for catalysis to proceed, a prediction confirmed by the recent report of the human $HGPRT_{ImmGP-PP_i-Mg}$ structure (*3*). Finally, this peptide bond is also cis in our *T. gondii* HGPRT−9-deazaguanine−PRPP−Mg^{2+} ternary complex (*27*).

Cis−Trans Isomerization. Thus, we are left with the inescapable conclusion that the Leu78−Lys79 peptide bond in *T. gondii* HGPRT (and the Leu67−Lys68 peptide bond in human HGPRT) exists in either the trans or cis configuration. We have discussed in the preceding article (*1*) several reasons why it is unlikely, for both HGPRTs, that this observation is an artifact of either the protein preparation or the specific crystallization conditions. Furthermore, we must distinguish between two possibilities concerning the cis versus trans nature of this peptide bond in HGPRT. Either the geometrical configuration of this bond is static, with some fraction of the enzyme molecules cis and the rest trans, or the peptide bond dynamically cycles between the cis and trans configurations during the course of catalysis. As discussed previously (*1*), the former possibility requires two populations of HGPRT molecules, one of which (trans) is inactive. This is contrary to observations with both human and *T. gondii* HGPRT. Therefore, we conclude that the Leu78−Lys79 peptide bond changes its geometric status during the course of catalysis.

We are aware of only one other example in which a particular non-proline peptide bond adopts either the cis or trans configuration, the Gly57−Asp58 peptide bond of flavodoxin from *Clostridium beijerinckii* (*30*). When the flavodoxin cofactor, flavin mononucleotide, is in the oxidized, quinone form, the peptide bond is cis. When the flavin is reduced to the semiquinone or hydroquinone form, the peptide bond adopts the trans geometry. And the energetics of isomerization of the Gly57−Asp58 peptide bond, as probed by site-directed mutagenesis, modulate the reduction potential of the flavin (*30*).

There are three possible mechanisms by which the Leu78−Lys79 peptide bond in *T. gondii* HGPRT converts between the cis and trans configurations. It either isomerizes spontaneously through a conformationally twisted amide (*31*, *32*), or is isomerized by protonation of the peptide NH of Lys79 by a general acid (*33*) or by nucleophilic attack on the carbonyl carbon of Leu78 (*32*). Isomerization of the peptide bond in *C. beijerinckii* flavodoxin appears to be spontaneous and rapid (*30*).

Role of Cis−Trans Peptide Bond Isomerization. We believe that isomerization of the Leu78−Lys79 peptide bond in HGPRT plays a critical role in the binding (trans → cis) of PRPP and the release (cis → trans) of pyrophosphate. We propose that a portion of the energy released upon PRPP binding to the apoenzyme is used to drive the Leu78−Lys79 peptide bond into the cis configuration, and that the energy released upon isomerization of the cis peptide bond back to the trans ground state helps to propel pyrophosphate out of the active site. For human HGPRT, the free energy change (ΔG) when PRPP binds to the apoenzyme is −7.9 kcal/mol (i.e., exothermic; $K_D = 1.3\ \mu M$ at 23 °C) (*7*). A non-proline cis peptide bond is about 2.5 kcal/mol destabilized relative to the trans configuration (*34*). So, if the Leu78−Lys79 peptide bond were cis rather than trans in the HGPRT apoenzyme, binding of PRPP would be more exothermic ($\Delta G = -10.4$ kcal/mol). In other words, the enzyme would fall into a deeper energy well upon binding PRPP. Similarly, when human HGPRT releases pyrophosphate from the HGPRT−IMP−PP_i complex, $\Delta G = 5.2$ kcal/mol ($K_D \sim 130\ \mu M$) (*7*). Were the peptide bond to remain cis during release of pyrophosphate, ΔG would increase to 7.7 kcal/mol, and the enzyme would have to climb out of a deeper energy well. By coupling a geometrical change in the protein with the binding and release of the pyrophosphate moiety, HGPRT is able to equalize the free energy changes as the reaction

coordinate is traversed (*35*), much in the same way that *C. beijerinckii* flavodoxin uses cis−trans isomerization to modulate the reduction potential of its cofactor (*36*). In this way, HGPRT avoids being trapped in a low-energy dead-end PRPP complex.

What does one make of $HGPRT_{IMP}$, then, in which the peptide bond is cis (*1*)? We think that it is possible that this structure has been forced into the higher-energy cis configuration by crystal packing interactions. The relationship between the core and hood domains in this structure most closely approaches that seen in $HGPRT_{XMP-PP_i-Mg}$. Also, several of the interactions between Lys79 and the hood domain are seen, although the extensive pyrophosphate-mediated network is missing. Therefore, we consider this structure to be, for now, the one exception to the rule exemplified by $HGPRT_{GMP}$, $HGPRT_{Apo}$, and both nucleotide complexes of human HGPRT. We are in the process of determining several other *T. gondii* HGPRT nucleotide complex and apoenzyme crystal structures, each in different unit cells (presumably with different packing interactions). These structures will provide us with a larger database from which to assess the geometry of the Leu78−Lys79 peptide bond.

Comprehensive HGPRT Reaction Mechanism

On the basis of our work and that of others, we can now propose a comprehensive, structure-based description of the conformational changes that occur during the HGPRT reaction. Our mechanism, which is illustrated in Figure 4, provides a unifying model on which further experiments can be based.

Six features of various HGPRT crystal structures contribute to our comprehensive reaction mechanism. First, the structure of HGPRT is now known at four points along the reaction coordinate: the apoenzyme (*5*, *37*), the bisubstrate complex (*2*, *26*, *27*), the biproduct complex (this article and ref *3*), and the nucleotide complex (*1*, *6*, *7*, *37*). Second, the coordination of pyrophosphate and Mg^{2+} by the enzyme shows that loops I and IV are tied together by an extensive hydrogen bond network when pyrophosphate or PRPP is bound in the active site. This network ties the hood domain onto the core domain in the lower part of the active site. Third, the Leu78−Lys79 peptide bond (loop I) is cis when pyrophosphate or PRPP is bound, but it is trans in the apoenzyme or the nucleotide complex. As discussed above, the energetics of the binding of PRPP and release of pyrophosphate become more favorable when they are coupled to isomerization of this peptide bond. Fourth, the purine binding site is disorganized and open in the apoenzyme (*1*, *5*). Fifth, loop III becomes ordered only when the enzyme binds ribose 5′-monophosphate. Sixth, when a previously unidentified active site loop, loop III′ (Thr180−Asn184 in *T. gondii* HGPRT), becomes ordered, it provides interactions that tie the upper part of the hood domain to the core domain (*1*).

Our mechanism also incorporates several key features of the kinetics of human HGPRT, the only HGPRT for which a complete description of the kinetic mechanism has been determined (*7*). First, the apoenzyme is incapable of binding hypoxanthine, and binds guanine only at high concentrations ($K_D > 200\ \mu M$). Accordingly, the reaction proceeds through ordered binding of the substrates, PRPP−Mg^{2+} first and purine second. The binding of PRPP by the HGPRT apoenzyme is confirmed by a dramatic PRPP-mediated stabilization against heat-induced denaturation (*38*). Second, release of PRPP from either the E−PRPP or E−PRPP−Hx complex is very slow (0.24 s^{-1}), indicative of a conformational change in the protein accompanying PRPP release. Third, chemical transfer of the phosphoribosyl group onto the purine is much more rapid than k_{cat} (131 vs 6 s^{-1}); the rate-determining step for the overall HGPRT-catalyzed reaction is the release of IMP, which is much slower than the release of pyrophosphate (>12 s^{-1}). The slow release of IMP has been interpreted previously as being due to a motion of loop II (*7*).

Step 1 of the Mechanism. In the apoenzyme, the residues that ligate the Mg^{2+} ions and their coordinating water molecules (Glu146, Asp147, and Asp206) are in the correct position and orientation to bind PRPP−Mg^{2+}. It is possible that HGPRT binds Mg^{1} before PRPP (*2*). Once the Leu78−Lys79 peptide bond adopts the cis configuration, PRPP is free to bind. From an energetic standpoint, the most favorable time for the peptide bond to isomerize would be at the same time as PRPP binding (Figure 4, panel 1). Loop III and the N-terminus of helix G adjust their positions to bind the 5′-phosphate of PRPP. The energetic cost of the disorder−order transition of loop III is likely readily offset by its extensive hydrogen bond interactions with the 5′-phosphate.

It has not been clear, however, why the purine cannot bind to the apoenzyme, although the purine-binding site is readily accessible to the purine base. Careful consideration of the structures, however, reveals the answer. In the apoenzyme, the main chain of Ile200, and the side chains of Ile148, Lys178, and Trp199, are not in the correct positions to make the specific binding interactions observed in either the bisubstrate complex, the biproduct complex, or the nucleotide complex. Instead, they are 1−3 Å displaced from these positions, leaving the purine binding site open and poorly ordered (*1*, *5*). For the purine to bind, these residues must adopt their correct positions. And to remain bound, the hood domain must close over the purine base. The interactions with the purine may be strong enough to organize these residues, but they are insufficient for achieving hood closure, in the absence of the link between the hood and the core provided by the pyrophosphate of PRPP. The purine can easily enter its binding site in the apoenzyme, but without the appropriate preorganization of the enzyme (caused by PRPP binding), it easily diffuses out of this binding site.

Step 2 of the Mechanism. Upon binding PRPP, the extensive network of salt bridges and hydrogen bonds that surrounds the pyrophosphate moiety forms in the lower active site, thereby drawing the core (loop I) and the hood (loop IV) close together on this side of the active site. Also, the two Mg^{2+} ions position the pyrophosphate moiety in the geometry needed for phosphoribosyl transfer to occur. Since there are no interactions between PRPP and the upper part of the hood domain (around Ile200), the hood is tied down at only one side. Thus, the upper active site is still open after PRPP binds. We predict that in the PRPP complex Lys178, β-strand 9, and Trp199 adopt positions similar to those found in the apoenzyme.

Step 3 of the Mechanism. The binding of the 5′-phosphate of PRPP causes loop III to become ordered (Figure 4, panel

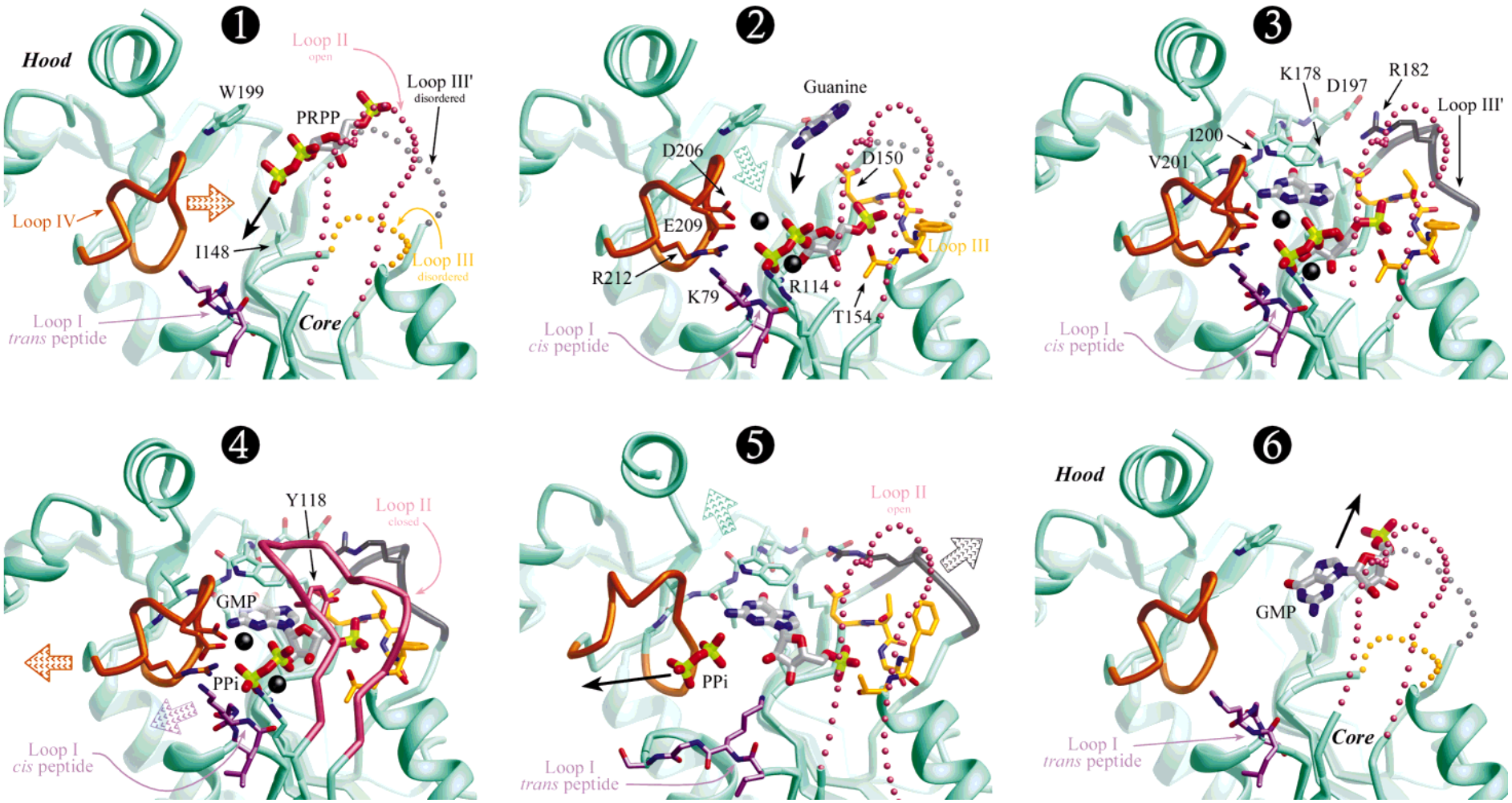

FIGURE 4: Motions that accompany HGPRT catalysis. The enzyme is shown in a RIBBONS (*21*) representation (green). The hood and core domains are at the upper left and lower right, respectively. Each active site loop is colored distinctly: loop I, lavender; loop II, rose; loop III, gold; loop III′, black; and loop IV, brown. Disordered (open) loops are shown as a series of spheres. (1) The apoenzyme. PRPP is entering the active site. The purine-binding clamp (Ile148 and Trp199) is open, as are loops II, III, and III′. The peptide bond between Leu78 and Lys79 in loop I is trans. Loop IV will close when PRPP is fully in the active site (arrow). (2) The PRPP complex. PRPP and the Mg^{2+} ions are bound, and thus, the peptide bond in loop I is now in the cis configuration. The interactions between the pyrophosphate moiety of PRPP, loop I, and loop IV are present, thereby closing the hood onto the core in the lower active site (see Figure 2). Loop III is ordered around the 5′-phosphate group. Guanine is entering the active site, after which the purine-binding clamp will close (arrow). (3) The bisubstrate complex. The purine-binding pocket is closed and ordered around the base. Closure of loop III (panel 2) has allowed loop III′ to close, placing Arg182 between Asp150 and Asp197. This closure completes the binding of the core and hood domains to one another. Closure of loop II will allow phosphoribosyl transfer to occur. (4) The biproduct complex. Loop II has closed, placing conserved residue Tyr118 in position to hydrogen bond to the 5′-phosphate group. Phosphoribosyl transfer occurred. Loops I and IV will now open to allow release of pyrophosphate (arrows). (5) The nucleotide complex. Pyrophosphate is leaving the active site, and the peptide bond in loop I has returned to the trans configuration. Loop II has opened. The upper active site (loop III′ and the hood domain) will now open to release GMP (arrows). (6) The apoenzyme. Loops III and III′ have opened, as has the hood, thereby allowing GMP to depart.

2). By ordering, loop III shifts Ile148 toward its proper position in the purine binding pocket, and it allows Asp150 to rise up toward Asp197, placing Asp150 in position to serve as the active site base. Solely by being ordered, loop III no longer prevents loop III′ from approaching the active site.

Step 4 of the Mechanism. Another source of confusion has been how the purine could bind after PRPP, since the purine binding pocket is located deeper in the active site cleft between the hood and core domains. However, examination of molecular models shows that, until the hood is closed at *both* the top and the bottom of the active site, the purine has sufficient room to enter the binding pocket. This point is underscored by the dramatic shift in the position of Trp199, in terms of both the location of the C^{α} and the orientation of the indole ring, between the apoenzyme and the complexes in which a purine is bound (*1*, *5*). As the purine binds (Figure 4, panels 2 and 3), it now causes the top of the hood to close down over the core. Residues Trp199 and Ile200 assume their proper positions. Either simultaneously with the purine entering its binding pocket, or shortly thereafter, loop III′ orders completely and extends the side chain of its conserved residue Arg182 toward prepositioned Asp150 (step 3) and Asp197, which lies at the beginning of β-strand 9 in the hood. This motion forms a tight double salt bridge, with the guanidinium of Arg182 sandwiched between the carboxylates of Asp150 and Asp197. This salt bridge, which is present in human $HGPRT_{ImmGP-PP_i-Mg}$ (*3*) and *T. gondii* $HGPRT_{dzG-PRPP-Mg}$ (*27*), locks the hood domain onto the core domain. It is telling, therefore, that *P. falciparum* HGPRT, which has a leucine residue in place of Arg182, is a very poor enzyme compared to *T. gondii* HGPRT. Finally, the ordered closure of the hood onto the core, first in the lower active site (step 2) and then in the upper active site (step 4), explains why the dissociation constants for the purine bases are extremely high ($K_D > 200$ μM), whereas the Michaelis constants are about 2 μM.

Step 5 of the Mechanism. The enzyme has one more motion it must make for catalysis to occur. Loop II must close over the ribose ring and the 5′-phosphate, making interactions between conserved Ser117 and Tyr118 and the 5′-phosphate group (Figure 4, panel 4). In human $HGPRT_{ImmGP-PP_i-Mg}$ and *T. gondii* $HGPRT_{dzG-PRPP-Mg}$, loop II is closed in all subunits. In the *T. cruzi* $HGPRT_{HPP-PRPP-Mg}$ crystal structure, however, both subunits contain similarly positioned Mg^{2+} ions, PRPP, and purine, but loop II is closed over the substrates in only *one* active site (*2*). This observation supports our proposal that closure of loop II is the final step preceding phosphoribosyl transfer. When loop II closes, a few additional hydrogen bonds are also made to the pyrophosphate group of PRPP. This final motion forces the two substrates to approach close enough to one another such that they then traverse the transition state. Mutation of the conserved Ser-Tyr dipeptide in loop II reduces k_{cat} by 100−1000-fold (*39*). These mutations likely alter the structure of loop II such that it cannot close tightly over the 5′-phosphate group. It is still not clear, however, whether loop II closure is absolutely required for catalysis (i.e., does a loop II deletion mutant possess activity?), or whether it just facilitates the reaction, in the manner described above.

Step 6 of the Mechanism. As discussed above, the detailed interactions between HGPRT and the pyrophosphate moiety differ between the various HGPRT ternary complex structures. The change in position between the ribose 5′-phosphate and the pyrophosphate groups before and after phosphoribosyl transfer alters and weakens the interactions between loop II and the reaction products, allowing loop II to return to the open position (Figure 4, panel 5).

Step 7 of the Mechanism. Pyrophosphate is now expelled from the active site, which is helped in part by the favorable energetics accompanying return of the cis peptide to the trans ground state (Figure 4, panel 5).

Step 8 of the Mechanism. Once pyrophosphate departs from the active site, the extensive network of hydrogen bonds that links the core and hood domains at the lower end of the HGPRT active site is lost, significantly weakening the ties that bind the two domains together (Figure 4, panel 5). The loss of pyrophosphate also weakens the interaction of loop IV (specifically Asp206) with the C^2-N^3 portion of the purine ring. The hood domain begins to loosen its grip on the purine base, pulling β-strand 9 and Trp199 away from the base. Nonetheless, it is important to realize that the nucleotide is still bound tightly by two distinct sets of interactions with the enzyme [the temperature factors for both the purine ring and the phosphate group are low, and the GMP $K_D = 7.1$ μM (*7*)], and loop III′ is still closed. Eventually, the interactions between Arg182 (loop III′) and Asp150 and Asp197 are broken, and loop III′ returns to its open position (Figure 4, panel 6).

Step 9 of the Mechanism. With loop III′ now open, loop III is finally free to be disordered upon departure of the 5′-phosphate. Accordingly, the nucleotide now leaves, and HGPRT returns to the apoenzyme conformational state (Figure 4, panel 6). These three sequential motions required for release of the nucleotide, namely, opening of the hood domain, opening of loop III′, and opening of loop III, explain why this is the rate-determining step in the HGPRT reaction mechanism.

Rate-Determining Step. The rate-determining step in the forward (nucleotide synthesis) reaction of HGPRT is release of nucleotide (NMP) from the enzyme−nucleotide complex (E−NMP), i.e., E−NMP → E + NMP (*7*), which is slower than the release of pyrophosphate from E−NMP−PP_i. Kinetics distinguished only between a few discrete states of the enzyme, namely, E + NMP, E−NMP, and E−NMP−PP_i. Therefore, the kinetic "single" rate-determining step actually consists of several elementary steps: conformational changes in the enzyme, specifically motion of active site loops and alteration in the spatial relationship between the hood and core domains; conformational changes in NMP; and actual dissociation of NMP. This more detailed distinction has recently been made for orotate phosphoribosyltransferase (*40*).

Examination of the HGPRT ternary complex structures in which loop II is closed shows that, for steric reasons, loop II must open before the NMP can dissociate from the HGPRT active site. As others have (*7*), let us assume for the moment that this opening of loop II is the slowest elementary step in the HGPRT reaction. By definition, therefore, *all* steps that precede or follow the opening of loop II *must* be faster than the opening of the loop itself. In particular, therefore, the dissociation of pyrophosphate from the loop II-closed complex and the dissociation of NMP from the loop II-open complex must both be faster than the opening of loop II itself:

$$E_{closed}-NMP-PP_i \xrightarrow{fast} E_{closed}-NMP + PP_i \xrightarrow{slow} E_{open}-NMP + PP_i \xrightarrow{fast} E + NMP + PP_i$$

But, in our structure of the biproduct complex, $HGPRT_{XMP-PP_i-Mg}$, loop II is *open*. We take this observation to be strong prima facie evidence that the opening of loop II *precedes* the release of pyrophosphate, and therefore that the slow step in NMP release *cannot* be the opening of loop II. Our original assumption that loop II opening is the rate-determining step of the overall reaction is wrong. Rather, one of the subsequent steps involved in NMP release must be rate-determining, i.e., hood opening, loop III′ opening, loop III opening,the conformational change of NMP, dissociation of NMP, or some combination of these.

ACKNOWLEDGMENT

We thank Prof. Beverly Davidson (The University of Michigan, Ann Arbor, MI) for supplying the human HGPRT clone. We are grateful for the expert assistance of Bob Sweet (National Synchrotron Light Source). D.W.B. expresses his heart-felt gratitude to his wife, Julie Bernstein, who has selflessly supported this and other work for many years. Without her support, possible only because she gave up her own successful science career to further his, this work would not have been possible.

REFERENCES

1. Héroux, A., White, E. L., Ross, L. J., and Borhani, D. W. (1999) *Biochemistry 38*, 14485−14494.
2. Focia, P. J., Craig, S. P., III, and Eakin, A. E. (1998) *Biochemistry 37*, 17120−17127.
3. Shi, W., Li, C. M., Tyler, P. C., Furneaux, R. H., Grubmeyer, C., Schramm, V. L., and Almo, S. C. (1999) *Nat. Struct. Biol. 6*, 588−593.
4. Sharma, V., Grubmeyer, C., and Sacchettini, J. C. (1998) S*tructure 6*, 1587−1599.
5. Schumacher, M. A., Carter, D., Roos, D. S., Ullman, B., and Brennan, R. G. (1996) *Nat. Struct. Biol. 3*, 881−887.
6. Eads, J. C., Scapin, G., Xu, Y., and Sachettini, J. C. (1994) *Cell 78*, 325−334.
7. Xu, Y., Eads, J., Sacchettini, J. C., and Grubmeyer, C. (1997) *Biochemistry 36*, 3700−3712.
8. Vasanthakumar, G., van Ginkel, S., and Parish, G. (1994) *Gene 147*, 153−154.
9. Davidson, B. L., Brown, J. E., Weber, C. E., Palella, T. D., and Roessler, B. J. (1993) *Gene 123*, 271−275.
10. Bradford, M. M. (1976) *Anal. Biochem. 72*, 248−254.
11. Gill, S. C., and von Hippel, P. H. (1989) *Anal. Biochem. 182*, 319−326.
12. Navaza, J. (1994) *Acta Crystallogr. A50*, 157−163.
13. Brünger, A. T., Kuriyan, J., and Karplus, M. (1987) *Science 235*, 458−460.
14. Rice, L. M., and Brünger, A. T. (1994) *Proteins: Struct., Funct., Genet. 19*, 277−290.
15. Jones, T. A., Zou, J. Y., Cowan, S. W., and Kjelgaard, M. (1991) *Acta Crystallogr. A47*, 110−119.
16. Murshudov, G. N., Vagin, A. A., and Dodson, E. J. (1997) *Acta Crystallogr. D53*, 240−255.
17. Lamzin, V. S., and Wilson, K. S. (1993) *Acta Crystallogr. D49*, 129−147.
18. Laskowski, R. A., MacArthur, M. W., Moss, D. S., and Thornton, J. M. (1993) *J. Appl. Crystallogr. 26*, 283−291.
19. Vriend, G. (1990) *J. Mol. Graphics 8*, 52−56.
20. Hooft, R. W. W., Vriend, G., Sander, C., and Abola, E. E. (1996) *Nature 381*, 272.
21. Carson, M. (1991) *J. Appl. Crystallogr. 24*, 958−961.
22. Lesch, M., and Nyhan, W. L. (1964) *Am. J. Med. 36*, 561−570.
23. Seegmiller, J. E., Rosenbloom, F. M., and Kelley, W. N. (1967) *Science 155*, 1682−1684.
24. Wilson, J. M., Stout, J. T., Pallela, T. D., Davidson, B. L., Kelley, W. N., and Caskey, C. T. (1986) *J. Clin. Invest. 77*, 188−195.
25. Lightfoot, T., Lewkonia, R. M., and Snyder, F. F. (1994) *Hum. Mol. Genet. 3*, 1377−1381.
26. Balendiran, G. K., Molina, J. A., Xu, Y., Torres-Martinez, J., Stevens, R., Focia, P. J., Eakin, A. E., Sacchettini, J. C., and Craig, S. P., III (1999) *Protein Sci. 8*, 1023−1031.
27. Héroux, A., White, E. L., Ross, L. J., and Borhani, D. W. (1999) (manuscript in preparation).
28. Li, C. M., Tyler, P. C., Furneaux, R. H., Kicska, G., Xu, Y., Grubmeyer, C., Girvin, M. E., and Schramm, V. L. (1999) *Nat. Struct. Biol. 6*, 582−587.
29. Steward, D. E., Sarkar, A., and Wampler, J. E. (1990) *J. Mol. Biol. 214*, 253−260.
30. Ludwig, M. L., Pattridge, K. A., Metzger, A. L., Dixon, M. M., Eren, M., Feng, Y., and Swenson, R. P. (1997) *Biochemistry 36*, 1259−1280.
31. Albers, M. W., Walsh, C. T., and Schreiber, S. L. (1990) *J. Org. Chem. 55*, 4984−4986.
32. Park, S. T., Aldape, R. A., Futer, O., DeCenzo, M. T., and Livingston, D. J. (1992) *J. Biol. Chem. 267*, 3316−3324.
33. Reimer, U., Mokdad, N. E., Schutkowski, M., and Fischer, G. (1997) *Biochemistry 36*, 13802−13808.
34. Ramachandran, G. N., and Mitra, A. K. (1976) *J. Mol. Biol. 107*, 85−92.
35. Albery, W. J., and Knowles, J. R. (1977) *Angew. Chem., Int. Ed. 16*, 285−293.
36. Hackney, D. D. (1990) Binding Energy and Catalysis, in *The Enzymes* (Sigman, D. S., and Boyer, P. D., Eds.) Vol. 19, pp 1−36, Academic Press, San Diego.
37. Somoza, J. R., Chin, M. S., Focia, P. J., Wang, C. C., and Fletterick, R. J. (1996) *Biochemistry 35*, 7032−7040.
38. Olsen, A. S., and Milman, G. (1977) *Biochemistry 16*, 2501−2505.
39. Jardim, A., and Ullman, B. (1997) *J. Biol. Chem. 272*, 8967−8973.
40. Wang, G. P., Cahill, S. M., Liu, X., Girvin, M. E., and Grubmeyer, C. (1999) *Biochemistry 38*, 284−295.

BI990508I